

A fast multipole boundary element method for solving two-dimensional thermoelasticity problems

Y. J. Liu · Y. X. Li · S. Huang

Received: 7 October 2013 / Accepted: 16 April 2014 / Published online: 3 May 2014
© Springer-Verlag Berlin Heidelberg 2014

Abstract A fast multipole boundary element method (BEM) for solving general uncoupled steady-state thermoelasticity problems in two dimensions is presented in this paper. The fast multipole BEM is developed to handle the thermal term in the thermoelasticity boundary integral equation involving temperature and heat flux distributions on the boundary of the problem domain. Fast multipole expansions, local expansions and related translations for the thermal term are derived using complex variables. Several numerical examples are presented to show the accuracy and effectiveness of the developed fast multipole BEM in calculating the displacement and stress fields for 2-D elastic bodies under various thermal loads, including thin structure domains that are difficult to mesh using the finite element method (FEM). The BEM results using constant elements are found to be accurate compared with the analytical solutions, and the accuracy of the BEM results is found to be comparable to that of the FEM with linear elements. In addition, the BEM offers the ease of use in generating the mesh for a thin structure domain or a domain with complicated geometry, such as a perforated plate with randomly distributed holes for which the FEM fails to provide an adequate mesh. These results clearly demonstrate the potential of the developed fast multipole BEM for solving 2-D thermoelasticity problems.

Keywords Fast multipole method · Boundary element method · 2-D thermoelasticity

Y. J. Liu (✉) · Y. X. Li · S. Huang
Mechanical Engineering, University of Cincinnati,
P.O. Box 210072, Cincinnati, OH 45221-0072, USA
e-mail: Yijun.Liu@uc.edu

Y. J. Liu
Institute for Computational Mechanics and Its Applications,
Northwestern Polytechnical University, Xi'an, Shaanxi 710072, China

1 Introduction

The boundary element method (BEM) has been applied to solve uncoupled steady-state thermoelasticity problems for more than three decades [1–6]. The BEM can be used to determine the deformation and stress fields in a structure under a thermal load. The thermal load, in the form of a change in temperature, is assumed to be given and its effect can be included in a domain integral in the boundary integral equation (BIE) formulation for thermoelasticity problems. This thermal term in the BIE can be converted to boundary integrals using different approaches [1–9]. Therefore, efficient boundary-only discretizations can be applied. As with the BEM for elastostatic problems, the thermoelasticity BEM has also been found especially effective in modeling thin structures, such as thin films and coatings, under thermal loads [10].

The fast multipole method [11–16] has been applied to accelerate the BEM for solving 2-D elastostatic problems, for example, by Fukui [17] and Liu [18] using complex variables, and by Yao et al. [19] using real variables in the multipole expansions. More applications of the 2-D fast multipole BEM for modeling porous, composite and functional-graded materials can be found in Ref. [16]. However, to the authors' best knowledge, the fast multipole BEM for solving 2-D thermoelasticity problems has not been reported in the literature.

In this work, uncoupled 2-D thermoelasticity problems are considered, for which the steady-state temperature field is assumed to be given and the thermal stress and displacement fields are sought. The thermal effect is included in the BIE by using the Galerkin vector [2, 10] and the domain integral is converted into boundary integrals. Therefore, only boundary integrals are present in the BIE. Fast multipole expansions and translations for the thermal term are derived and implemented based on the earlier fast multipole BEM for

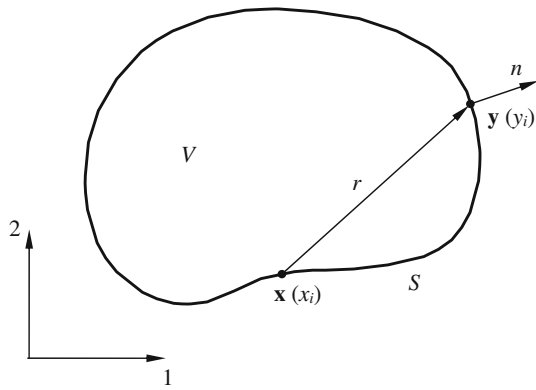


Fig. 1 Domain V and boundary S

2-D elastostatic BIE [18]. Constant line elements are used in the implementation and the direct integration of the kernels are done analytically so that all the nearly-singular integrals arising in modeling thin structure domains can be handled accurately. Several numerical examples are studied to verify the developed fast multipole BEM using analytical solutions or finite element method (FEM) solutions using linear and quadratic elements. Two thin-shape structures and a perforated plate with randomly distributed holes are included in the numerical study to show the accuracy and effectiveness of the BEM as compared with the FEM.

2 Fast multipole BEM formulation

The governing equations for a linear thermoelasticity problem in domain V (Fig. 1) with boundary S can be written as (index notation is used):

$$\sigma_{ij,j} = 0, \text{ in } V, \quad (1)$$

$$\sigma_{ij} = E_{ijkl} (\varepsilon_{kl} - \alpha\phi\delta_{kl}), \text{ in } V, \quad (2)$$

$$\varepsilon_{ij} = \frac{1}{2}(u_{i,j} + u_{j,i}), \text{ in } V, \quad (3)$$

where σ_{ij} , ε_{ij} and u_i are the stress, (total) strain and displacement field, respectively, E_{ijkl} is the elastic modulus tensor, α is the coefficient of thermal expansion, ϕ is the change of temperature, $(\)_{,i} = \partial(\)/\partial y_i$, and δ_{ij} is the Kronecker δ symbol. In this study, the mechanical body force is not considered and the temperature field ϕ is assumed to be known.

Applying the Somigliana's identity, we obtain the following direct BIE for 2-D thermoelasticity problems (we adopt the notation used in Refs. [2, 10]):

$$\begin{aligned} \frac{1}{2}u_i(\mathbf{x}) = & \int_S [U_{ij}(\mathbf{x}, \mathbf{y})t_j(\mathbf{y}) - T_{ij}(\mathbf{x}, \mathbf{y})u_j(\mathbf{y})]dS(\mathbf{y}) \\ & + C_0 \int_S [G_{ij,jk}(\mathbf{x}, \mathbf{y})n_k(\mathbf{y})\phi(\mathbf{y}) \\ & - G_{ij,j}(\mathbf{x}, \mathbf{y})q(\mathbf{y})]dS(\mathbf{y}), \quad \forall \mathbf{x} \in S, \end{aligned} \quad (4)$$

where t_i is the traction, $q = \partial\phi/\partial n$ is the heat flux, S is smooth around source point \mathbf{x} . The coefficient

$$\begin{aligned} C_0 = & \frac{1-2\nu}{2(1-\nu)}\gamma, \text{ with} \\ \gamma = & \frac{2(1+\nu)\mu\alpha}{1-2\nu} \quad (\text{for plane strain}), \end{aligned} \quad (5)$$

where ν is Poisson's ratio, and μ is the shear modulus.

The two kernel functions $U_{ij}(\mathbf{x}, \mathbf{y})$ and $T_{ij}(\mathbf{x}, \mathbf{y})$ in Eq. (4) are the displacement and traction components in the fundamental solution for 2-D problems (also called Kelvin's solution) given by the following expressions [16, 18]:

$$\begin{aligned} U_{ij}(\mathbf{x}, \mathbf{y}) = & \frac{1}{8\pi\mu(1-\nu)} \left[(3-4\nu)\delta_{ij} \log\left(\frac{1}{r}\right) \right. \\ & \left. + r_{,i}r_{,j} - \frac{1}{2}\delta_{ij} \right], \end{aligned} \quad (6)$$

$$\begin{aligned} T_{ij}(\mathbf{x}, \mathbf{y}) = & -\frac{1}{4\pi(1-\nu)r} \left\{ \frac{\partial r}{\partial n} [(1-2\nu)\delta_{ij} + 2r_{,i}r_{,j}] \right. \\ & \left. - (1-2\nu)(r_{,i}n_j - r_{,j}n_i) \right\}, \end{aligned} \quad (7)$$

for the plane strain case, in which $r = r(\mathbf{x}, \mathbf{y})$ is the distance between the source point \mathbf{x} and field point \mathbf{y} , n the outward normal (Fig. 1). Note that a constant term $-1/2\delta_{ij}$ in (6), which does not affect the solutions of the BIE, is added for the convenience in the multipole expansions of the kernels. The details of the multipole expansion will be described later. The Galerkin vector in Eq. (4) is given as follows [2, 10]:

$$G_{ij}(\mathbf{x}, \mathbf{y}) = \frac{1}{8\pi\mu} r^2 \log\left(\frac{1}{r}\right) \delta_{ij}, \quad (8)$$

and the U kernel can be represented by the Galerkin vector as:

$$U_{ij}(\mathbf{x}, \mathbf{y}) = G_{ij,kk}(\mathbf{x}, \mathbf{y}) - \frac{1}{2(1-\nu)} G_{ik,jk}(\mathbf{x}, \mathbf{y}). \quad (9)$$

Define

$$Q_i \equiv G_{ij,j} = -\frac{1}{8\pi\mu} (2\log r + 1) r r_{,i} \quad (10)$$

Then the thermal related term in BIE (4) (the second integral) can be written as:

$$b_i(\mathbf{x}) = C_0 \int_S \left[\frac{\partial Q_i(\mathbf{x}, \mathbf{y})}{\partial n(\mathbf{y})} \phi(\mathbf{y}) - Q_i(\mathbf{x}, \mathbf{y})q(\mathbf{y}) \right] dS(\mathbf{y}), \quad (11)$$

where

$$\frac{\partial Q_i(\mathbf{x}, \mathbf{y})}{\partial n(\mathbf{y})} = -\frac{1}{8\pi\mu} [(2\log r + 1)\delta_{ij} + 2r_{,i}r_{,j}] n_j. \quad (12)$$

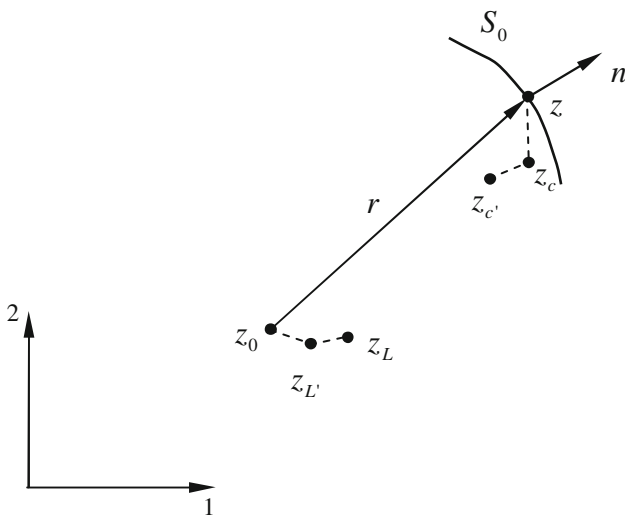


Fig. 2 Complex notation and the related points for fast multipole expansions

The fast multipole expansions and related translations for the integrals with the U and T kernels in BIE (4) are given in Refs. [16,18]. In the following, we only describe how to deal with the thermal term in the BIE with the fast multipole method.

To derive the fast multipole expansions for the thermal term, as shown in Eq. (11), we use the complex notation [15,16], which can simplify the derivations and improve the efficiency of computation. First, it is noticed that a complex representation of Q_i in Eq. (10) can be written as:

$$Q(z_0, z) = Q_1 + iQ_2 = \frac{1}{8\pi\mu} \left[\log(z_0 - z) + \overline{\log(z_0 - z)} + 1 \right] (z_0 - z), \quad (13)$$

where z_0 and z are the complex representation of source (collocation) point \mathbf{x} and field (integration) point \mathbf{y} , respectively (Fig. 2).

Starting with expression (13), we now present the multipole expansion, local expansion and their translations needed in the fast multipole BEM [15,16].

2.1 Multipole expansion (Moments)

Assuming z_c is a point close to the integration point z (Fig. 2), that is, $|z - z_c| \ll |z_0 - z_c|$ and for $k \geq 0$, we can derive the *multipole expansion* for the second integral in Eq. (11) on S_0 (Fig. 2) as follows:

$$\int_{S_0} Q(z_0, z)q(z)dS(z) = \frac{1}{8\pi\mu} \int_{S_0} \left[\log(z_0 - z) + \overline{\log(z_0 - z)} + 1 \right] (z_0 - z)q(z)dS(z) \quad (14)$$

$$= -\frac{1}{8\pi\mu} \int_{S_0} \left[\sum_{k=0}^{\infty} O_k(z_0 - z_c)I_k(z - z_c) + \sum_{k=0}^{\infty} \overline{O_k(z_0 - z_c)}I_k(z - z_c) - 1 \right] (z_0 - z)q(z)dS(z) = -\frac{1}{8\pi\mu} \left\{ [N_0(z_c) - z_0M_0(z_c)] - \sum_{k=0}^{\infty} O_k(z_0 - z_c) [N_k(z_c) - z_0M_k(z_c)] - \sum_{k=0}^{\infty} \overline{O_k(z_0 - z_c)} [\widetilde{N}_k(z_c) - z_0\overline{M}_k(z_c)] \right\},$$

where the three moments are given by:

$$M_k(z_c) = \int_{S_0} I_k(z - z_c)q(z)dS(z), \quad (15)$$

$$N_k(z_c) = \int_{S_0} I_k(z - z_c)zq(z)dS(z), \quad (16)$$

$$\widetilde{N}_k(z_c) = \int_{S_0} \overline{I_k(z - z_c)}zq(z)dS(z), \quad (17)$$

for $k \geq 0$, and the two auxiliary functions are defined by [15,16]:

$$I_k(z) = \frac{z^k}{k!}, \quad \text{for } k \geq 0,$$

$$O_0(z) = -\log(z); \text{ and } O_k(z) = \frac{(k-1)!}{z^k}, \text{ for } k \geq 1.$$

Note that $N_0(z_c)$ and $M_0(z_c)$ are in fact constants (not changing as z_c changes). Note also that moments $N_k(z_c)$ and $M_k(z_c)$ are related as shown in the following expression:

$$M_k(z_c) = \frac{1}{k} [N_{k-1}(z_c) - z_cM_{k-1}(z_c)], \quad (18)$$

for $k \geq 1$, which can be applied to calculate one of the two moments when the other has been obtained.

2.2 Moment-to-moment (M2M) translation

If point z_c is moved to a new location $z_{c'}$ (Fig. 2), the new moments can be obtained by using the *moment-to-moment translations*:

$$M_k(z_{c'}) = \sum_{l=0}^k I_{k-l}(z_c - z_{c'})M_l(z_c), \quad (19)$$

$$N_k(z_{c'}) = \sum_{l=0}^k I_{k-l}(z_c - z_{c'})N_l(z_c), \quad (20)$$

$$\widetilde{N}_k(z_c) = \sum_{l=0}^k \overline{I_{k-l}(z_c - z_c')} \widetilde{N}_l(z_c), \quad (21)$$

for $k \geq 0$, which are similar to those in the 2-D potential and elastostatic fast multipole BEM [15, 16].

2.3 Local expansion and moment-to-local (M2L) translation

If z_L is a point close to the source (collocation) point z_0 (Fig. 2), that is, $|z_0 - z_L| \ll |z_c - z_L|$. Expanding $\int_{S_0} Q(z_0, z) q(z) dS(z)$ about $z_0 = z_L$ and using Taylor series expansion, we obtain the following *local expansion*:

$$\begin{aligned} \int_{S_0} Q(z_0, z) q(z) dS(z) &= -\frac{1}{8\pi\mu} \left\{ (N_0 - z_0 M_0) \right. \\ &- \sum_{l=0}^{\infty} I_l(z_0 - z_L) [K_l(z_L) - z_0 L_l(z_L)] \\ &\left. - \sum_{l=0}^{\infty} \overline{I_l(z_0 - z_L)} [\widetilde{K}_l(z_L) - z_0 \overline{L}_l(z_L)] \right\}, \quad (22) \end{aligned}$$

where the local expansion coefficients are given by the following *M2L translations*:

$$L_l(z_L) = (-1)^l \sum_{k=0}^{\infty} O_{l+k}(z_L - z_c) M_k(z_c), \quad (23)$$

$$K_l(z_L) = (-1)^l \sum_{k=0}^{\infty} O_{l+k}(z_L - z_c) N_k(z_c), \quad (24)$$

$$\widetilde{K}_l(z_L) = (-1)^l \sum_{k=0}^{\infty} \overline{O_{l+k}(z_L - z_c)} \widetilde{N}_k(z_c), \quad (25)$$

for $l \geq 0$, which are similar to those in the 2-D potential and elastostatic cases [15, 16].

2.4 Local-to-local translation (L2L)

If the point for the local expansion is moved from z_L to $z_{L'}$ (Fig. 2), we can show that the new local expansion coefficients are given by the following *L2L translations*:

$$L_l(z_{L'}) = \sum_{m=l}^n I_{m-l}(z_{L'} - z_L) L_m(z_L), \quad (26)$$

$$K_l(z_{L'}) = \sum_{m=l}^n I_{m-l}(z_{L'} - z_L) K_m(z_L), \quad (27)$$

$$\widetilde{K}_l(z_{L'}) = \sum_{m=l}^n \overline{I_{m-l}(z_{L'} - z_L)} \widetilde{K}_m(z_L), \quad (28)$$

for $l \geq 0$, where n in the above expressions is the number of terms used in the first local expansion (about the point z_L).

Again, the translations are identical to those used in the 2-D potential and elastostatic cases [15, 16].

2.5 Expansions for the $\frac{\partial Q}{\partial n}$ Kernel integral

We now consider the complex representation and multipole expansion for the integral with the $\frac{\partial Q}{\partial n}$ kernel in Eq. (11). The complex notation for Eq. (12) can be written as:

$$\begin{aligned} \frac{\partial Q}{\partial n} &= \frac{\partial Q_1}{\partial n} + i \frac{\partial Q_2}{\partial n} \quad (29) \\ &= -\frac{1}{8\pi\mu} \left[\left(\log(z_0 - z) + \overline{\log(z_0 - z)} + 2 \right) n + \frac{z_0 - z}{z_0 - z} \bar{n} \right]. \end{aligned}$$

Thus, for the integral with the $\frac{\partial Q}{\partial n}$ kernel in Eq. (11), we have

$$\begin{aligned} \int_{S_0} \frac{\partial Q(z_0, z)}{\partial n} \phi(z) dS(z) &= -\frac{1}{8\pi\mu} \int_{S_0} \left\{ \left[\log(z_0 - z) + \overline{\log(z_0 - z)} + 2 \right] n \right. \\ &\quad \left. + \frac{z_0 - z}{z_0 - z} \bar{n} \right\} \phi(z) dS(z) \\ &= \frac{1}{8\pi\mu} \int_{S_0} \left\{ \left[\sum_{k=0}^n O_k(z_0 - z_c) I_k(z - z_c) \right. \right. \\ &\quad \left. \left. + \sum_{k=0}^n \overline{O_k(z_0 - z_c)} I_k(z - z_c) - 2 \right] n \right. \\ &\quad \left. - (z_0 - z) \bar{n} \sum_{k=0}^n \overline{O_{k+1}(z_0 - z_c)} I_k(z - z_c) \right\} \phi(z) dS(z) \\ &= \frac{1}{8\pi\mu} \left[-2P_0 + \sum_{k=0}^{\infty} O_k(z_0 - z_c) P_k(z_c) \right. \\ &\quad \left. + \sum_{k=0}^{\infty} \overline{O_k(z_0 - z_c)} \widetilde{P}_k(z_c) - z_0 \sum_{k=0}^{\infty} \overline{O_{k+1}(z_0 - z_c)} P_k(z_c) \right. \\ &\quad \left. + \sum_{k=0}^{\infty} \overline{O_{k+1}(z_0 - z_c)} R_k(z_c) \right], \quad (30) \end{aligned}$$

where the new multipole moments are:

$$P_k(z_c) = \int_{S_0} I_k(z - z_c) n \phi(z) dS(z), \quad (31)$$

$$\widetilde{P}_k(z_c) = \int_{S_0} \overline{I_k(z - z_c)} n \phi(z) dS(z), \quad (32)$$

$$R_k(z_c) = \int_{S_0} \overline{I_k(z - z_c)} z \bar{n} \phi(z) dS(z), \quad (33)$$

for $k \geq 0$. The M2M translations for these moments are:

$$P_k(z_{c'}) = \sum_{l=0}^k I_{k-l}(z_c - z_{c'}) P_l(z_c), \tag{34}$$

$$\tilde{P}_k(z_{c'}) = \sum_{l=0}^k \overline{I_{k-l}(z_c - z_{c'})} \tilde{P}_l(z_c), \tag{35}$$

$$R_k(z_{c'}) = \sum_{l=0}^k \overline{I_{k-l}(z_c - z_{c'})} R_l(z_c), \tag{36}$$

for $k \geq 0$. The local expansion and M2L translations are:

$$\int_{S_0} \frac{\partial Q(z_0, z)}{\partial n} \phi(z) dS(z) = \frac{1}{8\pi\mu} [-2P_0 + \sum_{l=0}^{\infty} I_l(z_0 - z_L) J_l(z_L) + \sum_{l=0}^{\infty} \overline{I_l(z_0 - z_L)} \tilde{J}_l(z_L) + z_0 \sum_{l=0}^{\infty} \overline{I_l(z_0 - z_L)} J_{l+1}(z_L) + \sum_{l=0}^{\infty} \overline{I_l(z_0 - z_L)} S_l(z_L)], \tag{37}$$

where

$$J_l(z_L) = (-1)^l \sum_{k=0}^{\infty} O_{l+k}(z_L - z_c) P_k(z_c), \tag{38}$$

$$\tilde{J}_l(z_L) = (-1)^l \sum_{k=0}^{\infty} \overline{O_{l+k}(z_L - z_c)} \tilde{P}_k(z_c), \tag{39}$$

$$S_l(z_L) = (-1)^l \sum_{k=0}^{\infty} \overline{O_{l+k+1}(z_L - z_c)} R_k(z_c), \tag{40}$$

for $l \geq 0$. The corresponding L2L translations are:

$$J_l(z_{L'}) = \sum_{m=l}^n I_{m-l}(z_{L'} - z_L) J_m(z_L), \tag{41}$$

$$\tilde{J}_l(z_{L'}) = \sum_{m=l}^n \overline{I_{m-l}(z_{L'} - z_L)} \tilde{J}_m(z_L), \tag{42}$$

$$S_l(z_{L'}) = \sum_{m=l}^n \overline{I_{m-l}(z_{L'} - z_L)} S_m(z_L), \tag{43}$$

for $l \geq 0$.

The details of the implementation of the fast multipole BEM for 2-D thermoelasticity are similar to that for 2-D elastostatic BIE [16, 18]. The only difference is that the new b vector in Eq. (11) due to the thermal load needs to be added to the right-hand side vector of the system of equations using the above fast multipole formulations. In this work, constant elements are used and all direct integrals are computed analytically (see Appendix) to avoid numerical integration. This is important for analyzing thin structures using the BEM [10, 20–23] where nearly-singular integrals can be troublesome if they are not computed correctly. Note that piecewise constant elements can give poor results when they are

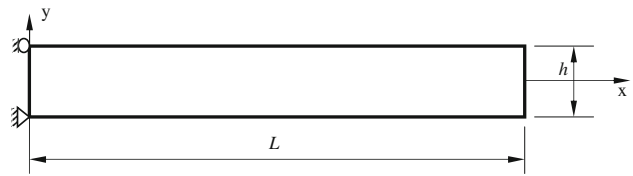


Fig. 3 A bar under different thermal loads ($L = 5$ m, $h = 1$ m), boundary conditions: $u_x = 0$ at $(0, h/2)$; $u_x = 0, u_y = 0$ at $(0, -h/2)$

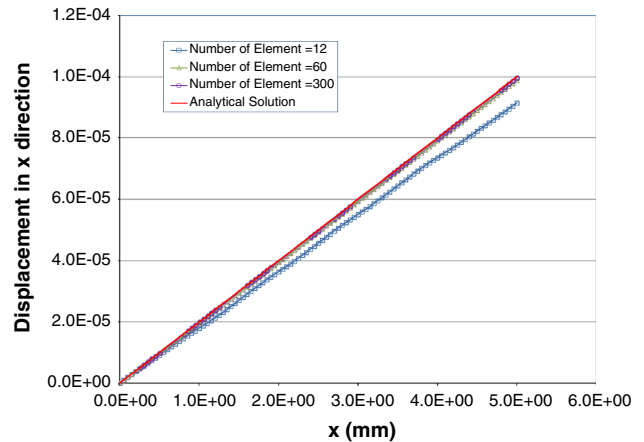


Fig. 4 BEM results with the constant thermal load

used to solve beam bending type of problems, because they cannot represent the rigid-body rotation on each element. A large number of elements will be needed to obtain reasonable results in the beam bending cases [24].

3 Numerical examples

We present five numerical examples to demonstrate the accuracy of the developed fast multipole BEM for solving 2-D thermoelasticity problems. All the computations were done on a desktop PC. In all the cases, the material has a Young’s modulus $E = 6.0$ GPa, Poisson’s ratio $\nu = 0.22$, and coefficient of thermal expansion $\alpha = 20.0 \times 10^{-6}/^\circ\text{C}$.

3.1 A bar under thermal loads

The first test for the BEM on the thermal stress analysis is a bar model (a plane stress problem) as shown in Fig. 3. First, a uniform temperature change $\phi = \Delta T = 1^\circ\text{C}$ is applied to the bar and the displacement field is calculated using the BEM. The results of the x -component of the displacement along the main axis of the bar are shown in Fig. 4 and compared with the analytical solution ($U_x = \alpha \Delta T x, 0 \leq x \leq 5$). Then a linear temperature change $\Delta T = x$ is applied to the bar and the same results are shown in Fig. 5 and compared with the analytical solution ($U_x = \alpha \Delta T x^2/2, 0 \leq x \leq 5$). Finally, a quadratic temperature change $\Delta T = x^2 - y^2$ is

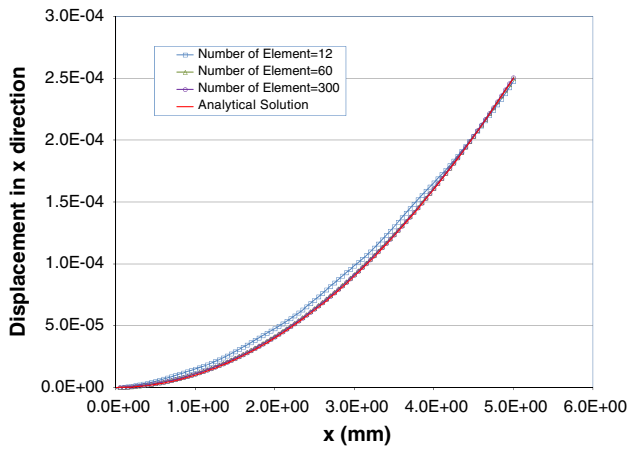


Fig. 5 BEM results with the linear thermal load

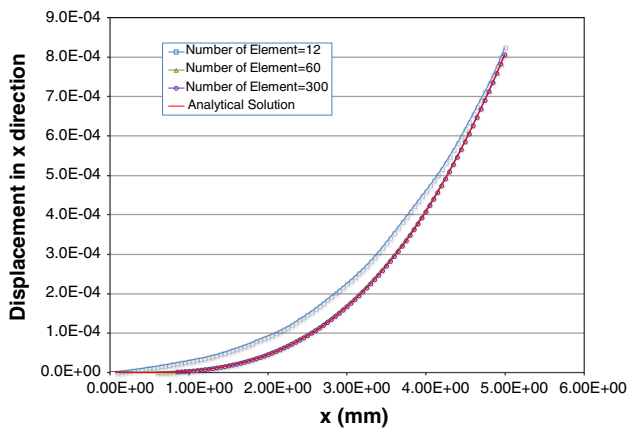


Fig. 6 BEM results with the quadratic thermal load

applied to the bar and the displacement results are shown in Fig. 6 and compared with the analytical solution ($U_x = \alpha \Delta T (x^3/3 - x/4), 0 \leq x \leq 5$). In all the three thermal loading cases, the BEM is observed to deliver satisfactory results with only 60 constant boundary elements.

3.2 Thin coating on a rigid cylinder

The coating on a rigid cylinder (a plane strain problem), as shown in Fig. 7, is studied next using the developed BEM. The annular region has an outer radius $a = 10.1$ m and an inner radius $b = 10$ m. A uniform temperature change $\Delta T = 100$ °C is applied to the coating. Under these conditions, the analytical solution of the radial displacement at the outer boundary is found to be:

$$u_r = \frac{\alpha \Delta T a}{2} \left(1 - \frac{b^2}{a^2}\right) \frac{1 + \nu}{1 - \nu} \left[1 + \frac{1 - 2\nu}{1 + (1 - 2\nu) \frac{b^2}{a^2}} \left(1 - \frac{b^2}{a^2}\right)\right]. \quad (44)$$

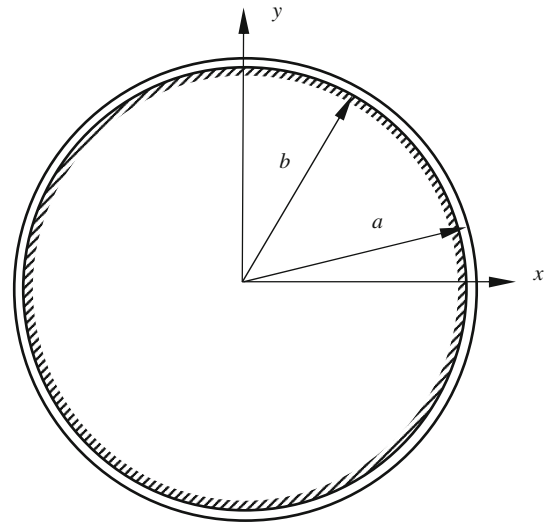


Fig. 7 Coating on a rigid cylinder ($a = 10.1$ m, $b = 10$ m), boundary conditions: $u_x = 0, u_y = 0$ on the inner boundary ($r = b$)

Several BEM discretizations are used with the number of boundary elements increasing from 40 to 5,000 and compared with the FEM (ANSYS® Q4 (linear, quadrilateral 4-node) elements). The obtained BEM and FEM results for the radial displacement and stress components on the outer boundary of the coating are shown in Table 1 and compared with the analytical solution in Eq. (44). Both the BEM and FEM give very good results in this case. As shown in the table, when the number of boundary elements is 200, the relative errors of radial displacement (u_r) and circumferential stress (σ_θ) of the BEM results are already less than 1%.

3.3 Coating on a 2D gear model

The coating on a 2D gear model (a plane stress problem), as shown in Fig. 8, is studied next. The coating is applied with a uniform temperature change $\Delta T = 100$ °C. Both the BEM and FEM with Q8 (quadrilateral, quadratic 8-node) elements are applied. The FEM mesh on one tooth is shown in Fig. 9. The BEM results at point A near the center of the tooth shown in Fig. 9 are compared with the FEM results as shown in Table 2. It is observed that all the BEM and FEM displacement and stress component results are converged, except for the FEM stress component in the y-direction in the FEM results. Due to the limitation of the ANSYS® academic license, no larger FEM models could be attempted.

3.4 A perforated plate model with uniformly distributed holes

A perforated plate with 7×7 (a total of 49) uniformly distributed holes (a plane stress problem) as shown in Fig. 10

Table 1 Comparison of BEM and FEM results for the thin coating model

Method	Number of elements	Degrees of freedom	u_r (m)	σ_θ (Pa)
FEM (Q4 elements)	16	64	3.1203E-04	-1.5256E + 07
	80	320	3.1343E-04	-1.5228E + 07
	403	1,598	3.1288E-04	-1.5139E + 07
	4,405	11,730	3.1349E-04	-1.5202E + 07
BEM (constant elements)	40	80	3.0979E-04	-1.4790E + 07
	200	400	3.1342E-04	-1.5131E + 07
	1,000	2,000	3.1330E-04	-1.5149E + 07
	5,000	10,000	3.1346E-04	-1.5151E + 07
Analytical			3.1349E-04	-1.5189E + 07

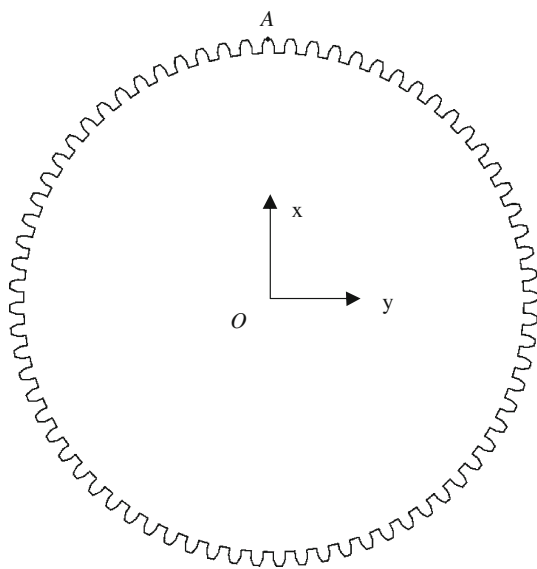


Fig. 8 Coating on a 72-tooth rigid gear model (pitch diameter = 10 m, coating thickness = 0.1 m, point A at (-0.0674745, 13.09235), boundary conditions: $u_x = 0, u_y = 0$ along the gear and coating interface)

is considered in this case. A uniform temperature change $\Delta T = 100\text{ }^\circ\text{C}$ is applied to the plate which is fixed along all the four outside edges. The computed results using the BEM and FEM (with Q8 element) at point B are listed in Table 3. It is observed that the BEM and FEM results for the x-component of displacement and y-component of stress are converged and agree with each other. However, the y displacement and shear stress using both methods are not yet converged when the number of elements increases. This is because point B lies on the horizontal symmetric axis of the plate, and the results of the y-displacement and shear stress should be close to zero. Indeed these values are very small compared with the other components of displacement and stress. In Fig. 11 the computed x-component displacement on the edge of the center hole are plotted, where the BEM



Fig. 9 FEM mesh for the coating on one tooth of the gear model

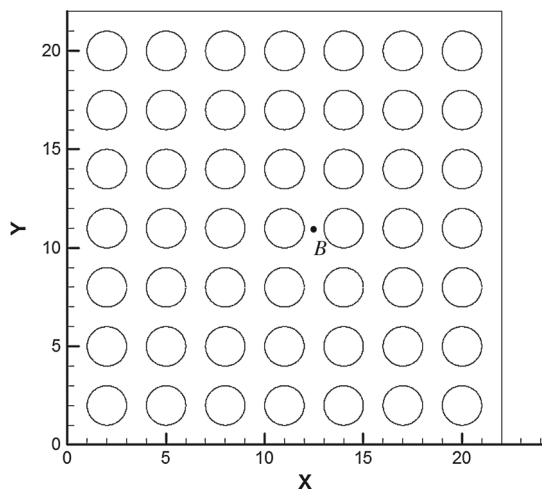
and FEM results are shown to agree very well. In Figs. 12 and 13, the contour plots of the x-component displacement and stress using the BEM are shown, which show the symmetry in the results as expected from this case.

3.5 A perforated plate model with randomly distributed holes

Finally, a perforated plate with 7×7 (a total of 49) randomly distributed holes (a plane stress problem) as shown in Fig. 14 is considered. A uniform temperature change $\Delta T = 100\text{ }^\circ\text{C}$ is applied to the plate which is fixed along all the edges. Unfortunately, in this case, it is impossible to mesh the plate with ANSYS[®] because some holes are very close to each other and the model requires very fine mesh in the narrow regions. Thus, BEM is the only method used to obtain the results. The contour plots of the x-component displacement

Table 2 Comparison of the BEM and FEM results for the gear coating model

Method	Element size	Degrees of freedom	Displacement and stress at point A				
			u_x (m)	u_y (m)	σ_x (Pa)	σ_y (Pa)	τ_{xy} (Pa)
BEM (constant elements)	1.00E-02	16, 848	-5.6770E-07	2.4332E-05	-1.1341E+07	-5.4191E+03	-2.4732E+05
	1.00E-03	152, 640	-5.7394E-07	2.4332E-05	-1.1476E+07	-5.4638E+03	-2.5040E+05
	5.00E-04	304, 704	-5.7417E-07	2.4332E-05	-1.1476E+07	-5.4640E+03	-2.5041E+05
	3.05E-04	499, 104	-5.7420E-07	2.4332E-05	-1.1476E+07	-5.4641E+03	-2.5042E+05
FEM (Q8 elements)	1.00E-02	16, 850	-5.7716E-07	2.4564E-05	-1.1573E+07	2.3004E+05	-2.4814E+05
	5.00E-03	49, 096	-5.6780E-07	2.4344E-05	-1.1477E+07	5.1027E+04	-2.4735E+05
	1.50E-03	403, 038	-5.7445E-07	2.4333E-05	-1.1477E+07	2.9332E+03	-2.4965E+05
	1.46E-03	446, 696	-5.7486E-07	2.4333E-05	-1.1477E+07	1.4943E+03	-2.4978E+05

**Fig. 10** A perforated plate model with uniformly distributed holes (plate side length = 22 m, radius of holes = 1 m, point B at (12.5, 11.0), boundary conditions: $u_x = 0, u_y = 0$ on all the four outside straight edges)

and stress are shown in Figs. 15 and 16, respectively. The displacement and stress results at point C are shown in Table 4. In this case, the BEM does not need any special treatment on the meshing part when modeling the perforated plate with randomly distributed holes.

4 Discussions

In this work, the fast multipole BEM for 2-D elastostatic problems is extended to the 2-D thermoelasticity case. The thermal load term in the BIE, or the new right-hand side vector in the BEM system of equations, is calculated using the fast multipole method. The multipole expansion, local expansion and their corresponding translations for the thermal term are presented in this paper for the first time. Numerical examples show the accuracy and effectiveness of the developed fast multipole BEM for the thermoelasticity analysis of 2-D structures, especially thin structures or structures

Table 3 Comparison of results at point B from BEM and FEM

Method	Element size	Degrees of freedom	Displacement and stress at point B				
			u_x (m)	u_y (m)	σ_x (Pa)	σ_y (Pa)	τ_{xy} (Pa)
BEM (constant elements)	0.1257	6, 300	-9.0746E-05	2.4936E-07	-3.9377E+06	-1.7971E+07	3.2208E+04
	0.0251	31, 500	-9.0540E-05	-5.7575E-08	-3.9120E+06	-1.8057E+07	2.4074E+03
	0.01	157, 500	-9.0532E-05	5.4860E-09	-3.9055E+06	-1.8071E+07	-3.6188E+01
	0.005	787, 500	-9.0581E-05	-3.0541E-09	-3.7997E+06	-1.8072E+07	-6.5026E-01
	0.0016	1575, 000	-9.0548E-05	9.4539E-10	-3.8853E+06	-1.8065E+07	1.1551E+00
FEM (Q8 elements)	0.2	53, 036	-9.0527E-05	-1.6652E-09	-3.9027E+06	-1.8063E+07	-1.2917E+00
	0.1	213, 026	-9.0535E-05	-3.1307E-09	-3.9062E+06	-1.8063E+07	-5.1610E+00
	0.065	481, 674	-9.0538E-05	-3.4652E-09	-3.9067E+06	-1.8063E+07	-5.0363E+00

Fig. 11 Plot of u_x on the edge of the center hole in the plate (BEM has 6300 DOFs and FEM has 213026 DOFs)

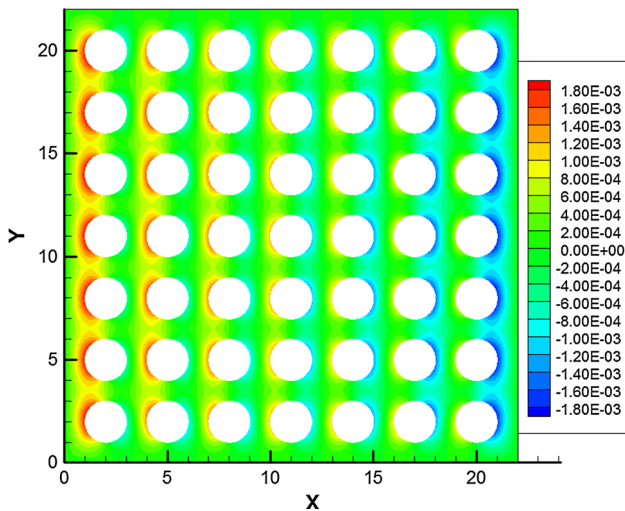
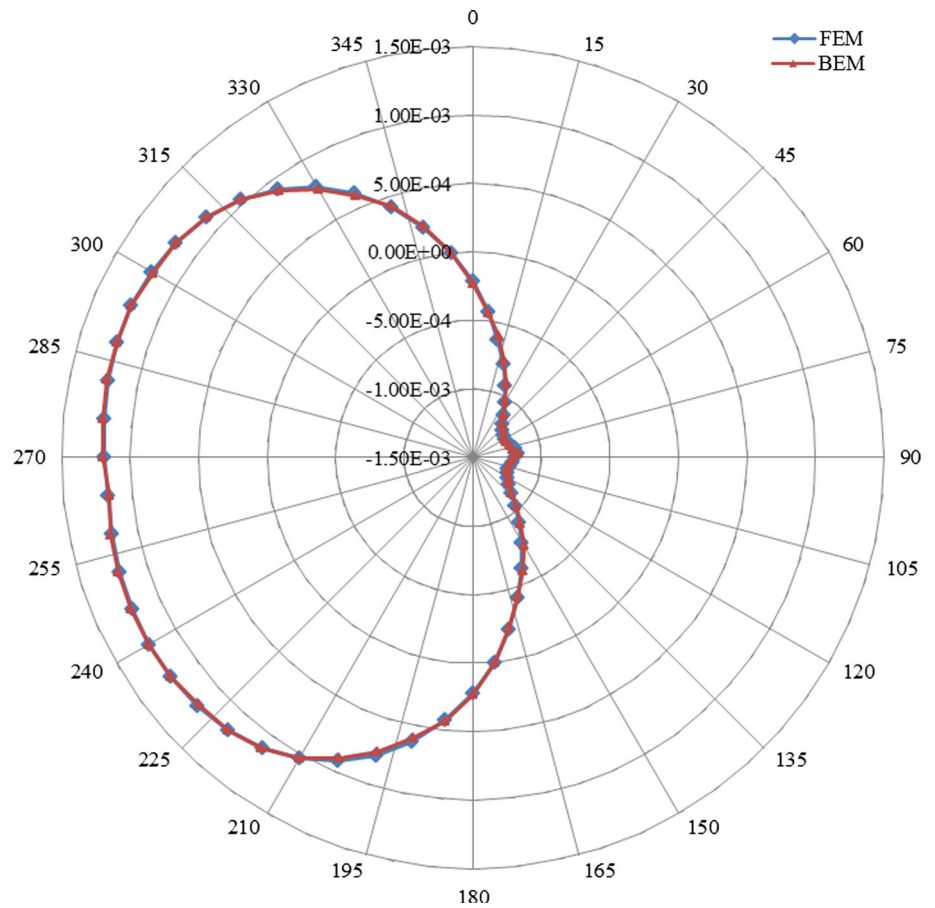


Fig. 12 Contour plot of u_x (BEM, 157500 DOFs)

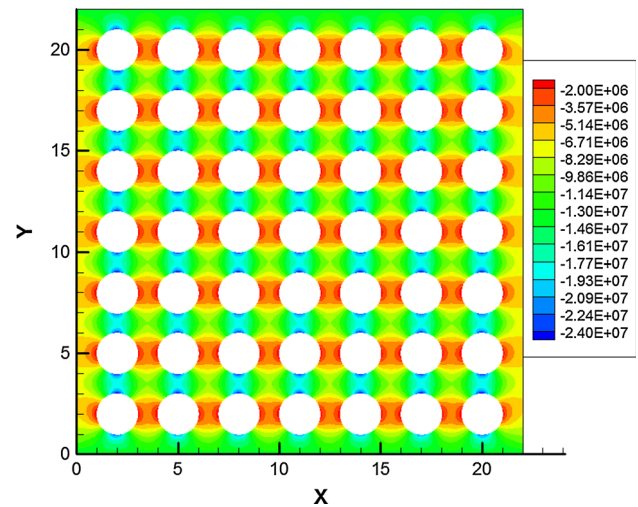


Fig. 13 Contour plot of σ_x (BEM, 157500 DOFs)

with complicated geometries which are difficult for the FEM to handle because meshing of the domain can be challenging and time consuming.

Although the BEM is much easier in meshing and accurate in analysis, the efficiency in computation still lags compared

with the FEM in solving a comparable model with the same level of accuracy, even with the fast multipole method. Therefore, further improvement in the algorithms and optimization of the code need to be investigated. For stress analysis problems, it is beneficial to apply high-order boundary elements,

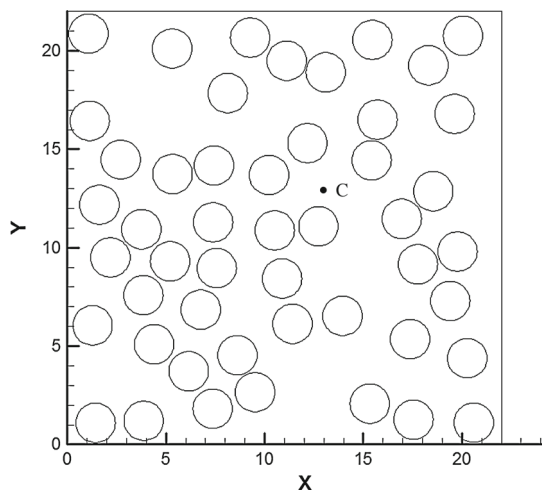


Fig. 14 A perforated plate model with randomly distributed holes (plate side length = 22 m, radius of holes = 1 m, boundary conditions: $u_x = 0$, $u_y = 0$ on all four outside straight edges)

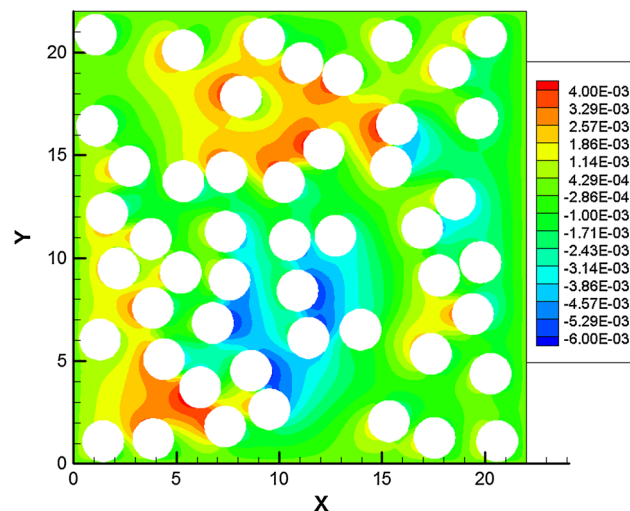


Fig. 15 Contour plot of u_x (BEM, 101440 DOFs)

such as quadratic elements, so that a much smaller number of elements can be used to solve the problem with the same or higher accuracy, when compared with the current implementation using the constant elements.

Table 4 BEM results at point *C* for the plate with randomly distributed holes

Degrees of freedom	Displacement and stress at point (13.2, 13.2)				
	u_x (m)	u_y (m)	σ_x (Pa)	σ_y (Pa)	τ_{xy} (Pa)
6,340	-8.2422E-04	5.7292E-04	-1.0154E+07	8.1175E+06	1.8518E+06
12,680	-1.0492E-03	5.1055E-04	-1.0052E+07	8.0990E+06	1.8709E+06
25,360	-1.0467E-03	5.1797E-04	-1.0048E+07	8.1031E+06	1.8633E+06
50,720	-1.0454E-03	5.2151E-04	-1.0046E+07	8.1055E+06	1.8595E+06
1,01,440	-1.0448E-03	5.2326E-04	-1.0045E+07	8.1068E+06	1.8575E+06

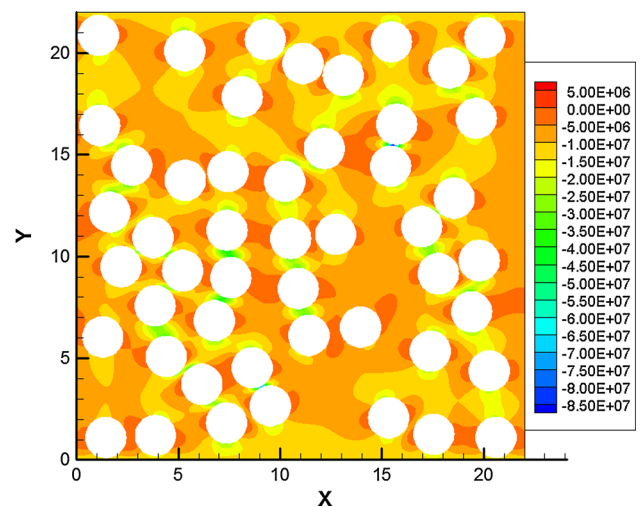


Fig. 16 Contour plot of σ_x (BEM, 101440 DOFs)

A multi-domain version of the developed fast multipole BEM can be applied to solve thermal stresses and interface cracks in multi-layered thin films and coatings. It can also be extended to the 3-D thermoelasticity BIE to study more realistic 3-D models under the thermal load. Fracture mechanics problems of cracks in structures under a thermal load can also be studied using the fast multipole BEM. Coupled thermal and elasticity problems can also be attempted using the fast multipole BEM. Other fast solution methods, such as the adaptive cross approximation method [25,26], can be applied, which may be easier to implement than the fast multipole BEM.

Acknowledgments The authors would like to thank one of the anonymous reviewers of the manuscripts for pointing out the relation as shown in Eq. (18) between the two moments.

Appendix: analytical integration of the thermal related kernels

The integrations of the two thermal related kernels in Eq. (11) on a constant element or line segment ΔS shown in Fig. 17

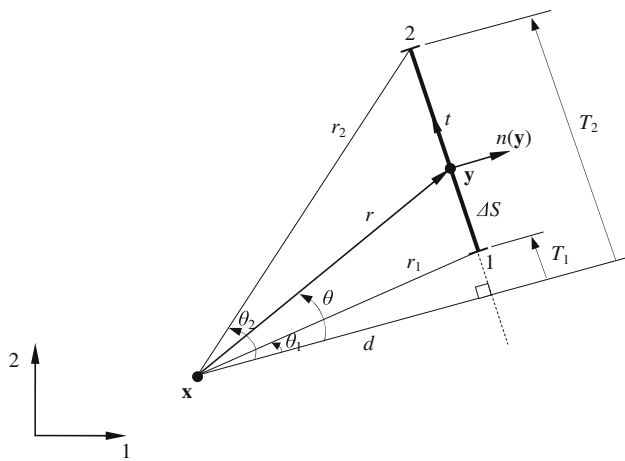


Fig. 17 Analytical integration on a constant element

(from point 1 to point 2) can be evaluated analytically as follows (see also Appendix A of Ref. [16] for the analytical integration of other kernels). First, we define:

$$J_i \equiv \int_{\Delta S} Q_i dS = \frac{1}{8\pi\mu} \int_{\Delta S} \left[2 \log \left(\frac{1}{r} \right) - 1 \right] r r_{,i} dS, \quad (45)$$

$$K_i \equiv \int_{\Delta S} \frac{\partial Q_i}{\partial n} dS = \frac{1}{8\pi\mu} \int_{\Delta S} \left[\left(2 \log \left(\frac{1}{r} \right) - 1 \right) n_i - 2 r_{,i} \frac{\partial r}{\partial n} \right] dS, \quad (46)$$

for $i = 1$ and 2 .

In the local coordinate system $n - t$ at \mathbf{y} on ΔS (Fig. 17), we have

$$J_1^{(n-t)} = \frac{d}{8\pi\mu} [2I_0 - (T_2 - T_1)], \quad (47)$$

$$J_2^{(n-t)} = \frac{1}{8\pi\mu} [r_1^2 \log r_1 - r_2^2 \log r_2], \quad (48)$$

$$K_1^{(n-t)} = \frac{1}{8\pi\mu} [2I_0 - (T_2 - T_1) - 2d(\theta_2 - \theta_1)], \quad (49)$$

$$K_2^{(n-t)} = \frac{d}{4\pi\mu} \log \left(\frac{r_1}{r_2} \right), \quad (50)$$

where

$$I_0 = -d(\theta_2 - \theta_1) + (T_2 - T_1) - T_2 \log r_2 + T_1 \log r_1. \quad (51)$$

Applying the transformation for vectors in 2-D, we obtain the results for J_i and K_i in the global coordinate system.

References

1. Rizzo FJ, Shippy DJ (1977) An advanced boundary integral equation method for three-dimensional thermoelasticity. *Int J Numer Methods Eng* 11:1753–1768

2. Brebbia CA, Dominguez J (1989) *Boundary elements—an introductory course*. McGraw-Hill, New York

3. Banerjee PK (1994) *The boundary element methods in engineering*, 2nd edn. McGraw-Hill, New York

4. Kane JH (1994) *Boundary element analysis in engineering continuum mechanics*. Prentice Hall, Englewood Cliffs

5. Becker AA (1992) *The boundary element method in engineering*. McGraw-Hill, New York

6. Aliabadi MH (2002) *The boundary element method—applications in solids and structures*, vol 2. Wiley, Chichester

7. Sládek V, Sládek J (1983) Boundary integral equation method in thermoelasticity part I: general analysis. *Appl Math Model* 7:241–253

8. Cheng AHD, Chen CS, Golberg MA, Rashed YF (2001) BEM for thermoelasticity and elasticity with body force—a revisit. *Eng Anal Bound Elem* 25:377–387

9. Matsumoto T, Guzik A, Tanaka M (2005) A boundary element method for analysis of thermoelastic deformations in materials with temperature dependent properties. *Int J Numer Methods Eng* 64:1432–1458

10. Chen XL, Liu YJ (2001) Thermal stress analysis of multi-layer thin films and coatings by an advanced boundary element method. *CMES. Comput Model Eng Sci* 2:337–350

11. Rokhlin V (1985) Rapid solution of integral equations of classical potential theory. *J Comput Phys* 60:187–207

12. Greengard LF, Rokhlin V (1987) A fast algorithm for particle simulations. *J Comput Phys* 73:325–348

13. Greengard LF (1988) *The rapid evaluation of potential fields in particle systems*. The MIT Press, Cambridge

14. Nishimura N (2002) Fast multipole accelerated boundary integral equation methods. *Appl Mech Rev* 55:299–324

15. Liu YJ, Nishimura N (2006) The fast multipole boundary element method for potential problems: a tutorial. *Eng Anal Bound Elem* 30:371–381

16. Liu YJ (2009) *Fast multipole boundary element method—theory and applications in engineering*. Cambridge University Press, Cambridge

17. Fukui T (1998) *Research on the boundary element method—development and applications of fast and accurate computations*. Ph.D. Dissertation (in Japanese), Department of Global Environment Engineering, Kyoto University

18. Liu YJ (2006) A new fast multipole boundary element method for solving large-scale two-dimensional elastostatic problems. *Int J Numer Methods Eng* 65:863–881

19. Yao ZH, Kong F, Wang H, Wang P (2004) 2D simulation of composite materials using BEM. *Eng Anal Bound Elem* 28:927–935

20. Liu YJ (1998) Analysis of shell-like structures by the boundary element method based on 3-D elasticity: formulation and verification. *Int J Numer Methods Eng* 41:541–558

21. Luo JF, Liu YJ, Berger EJ (1998) Analysis of two-dimensional thin structures (from micro- to nano-scales) using the boundary element method. *Comput Mech* 22:404–412

22. Luo JF, Liu YJ, Berger EJ (2000) Interfacial stress analysis for multi-coating systems using an advanced boundary element method. *Comput Mech* 24:448–455

23. Chen XL, Liu YJ (2005) An advanced 3-D boundary element method for characterizations of composite materials. *Eng Anal Bound Elem* 29:513–523

24. Liu YJ, Li YX (2014) Slow convergence of the BEM with constant elements in solving beam bending problems. *Eng Anal Bound Elem* 39:1–4

25. Bebendorf M (2008) Hierarchical matrices: a means to efficiently solve elliptic boundary value problems. Springer, Berlin

26. Rjasanow S, Steinbach O (2007) *The fast solution of boundary integral equations*. Springer, Berlin